# RSC Advances

ROYAL SOCIETY
OF CHEMISTRY

www.rsc.org/advances

# Imaging the strain induced carbon black filler network structure breakage with nano X-ray tomography

Weiming Zhou [a], Liang Chen [*][a], Jie Lu [a], Zeming Qi [a], Ningdong Huang [a],

Liangbin Li*[a], Wanxia Huang [b]

*a National Synchrotron Radiation Lab and College of Nuclear Science and Technology, CAS Key*

*Laboratory of Soft Matter Chemistry, University of Science and Technology of China, Hefei, China*

*b Beijing Synchrotron Radiation Facility, Institute of High Energy Physics, Chinese Academy of Sciences, Beijing,*

*China*

## Abstract

Aiming to study the mechanical enhancement by filler network in rubber composite, three-dimensional images are acquired with in-situ full field transmission X-ray microscopy (TXM), the network structure of carbon black (CB) aggregates in rubber matrix is studied with and without strain. Statistical analysis shows that the frequency of similar-sized aggregates decreases with the increase of aggregate size as well as the inter-aggregate distance monotonically without strain. An oscillation of the frequency-size plot is induced by strain on top of the damping trend, which is interpreted as stretch-induced breakage and re-aggregation of CB aggregates. Calculation adopting a soft-hard network model, predict a reduction of the contribution of CB network to the mechanical property of rubber composite by about 60% caused by the breakage and re-aggregation of CB aggregates compared to that without strain. The experimental results direct prove the structural origin of Payne

[*] rychen@ustc.edu.cn, lbli@ustc.edu.cn

effect and also show that TXM is a valuable tool to study the mechanical

enhancement mechanism of filled rubber composites.

## Introduction

Natural rubber is one of the most fascinating and important industrial polymers, which is irreplaceable in many important and key areas due to its excellent mechanical properties. In addition to polymer molecules, inorganic nanofillers like carbon black (CB), silica and $CaCO_3$ are almost inevitably added in commercial rubber products, where filler network provides an important contribution to the mechanical performance of rubber composites.[1-9] Though the importance of filler network has been well recognized since the dawn of rubber industry, the mechanism of mechanical enhancement is still not completely understood yet. Some specific mechanical behaviors like the well-known Payne effect,[10-12] are considered to be related to breakage and recovery of the fillers network during the deformation process. Unfortunately, due to the peculiar length scales of filler network (from hundreds nanometer to micrometer),[13] the structure information of fillers in un-deformed rubber stay scarce, not to mention that under deformation condition. Advanced in-situ techniques with the capability to probe filler network become critical for unveiling the mechanism of mechanical enhancement of filler.

Several techniques with different advantages and disadvantages have been used to study the fillers network structure in rubber matrix. Primary CB particles with size of tens of nanometer generally gather into aggregates or agglomerates with size larger than 100 nm. For visible light microscopy[14], it is difficult to detect the filler particles and aggregates because of the limitations of its spatial resolution and penetrability. While for atomic force microscope (AFM)[15-17] and scanning electron microscope

(SEM)[18, 19], can obtain the fillers network structure on the surface of the rubber matrix with high spatial resolution, but the network structure inside the rubber matrix cannot be detected. There is no denying that transmission electron microscopy (TEM) can obtain the network structure in the rubber matrix with high spatial resolution[20-23], but the weak penetrability of electron makes it troublesome both in the sample process and image process. The samples must be cut into ultra-thin pieces, which increase the difficulties in imaging and cause the filler particles losing during the slicing process. Moreover, the severe imaging circumstance of TEM makes it difficult to follow the deformation of network structure during stretching process. Ultra-small angle X-ray scattering (U-SAXS)[24, 25] is a useful technique for in-situ studying, enabling structural studies in a large length scale range from nanometer to micrometer and extreme experimental environment, but the result is statistical and model-dependence, in which local structure change is difficult to be obtained. All of the techniques mentioned above seem unable to obtain the three-dimensional (3D) network structure in the large field with high resolution, which is the essential parameter in building the enhancement mechanism for filled rubber composites.

As an established synchrotron radiation technique, full field transmission X-ray microscopy (TXM)[26, 27] provides not only high spatial resolution (20-50 nm), but also the high penetrability of X-rays through bulk sample for structural information within large volume, which has been widely used in many research fields, such as archaeology[28], composite materials,[29] pharmacy,[30] and *etc*. Meanwhile, TXM is a non-destructive probe, suitable for in-situ detection on structural evolution during

mechanical test and consequently beneficial to the establishment of the relationship between fillers network structure and mechanical properties of rubber composites. Unfortunately, few works have been performed with TXM to study the CB dispersion in the rubber matrix in any reported research to our knowledge.

In this work, the 3D dispersion of CB aggregates in natural rubber matrix under strain of 0 and 3 are studied with synchrotron radiation TXM, where size and dispersion of the aggregates are extracted from the 3D images. Some important phenomena are found, including nano pores generating due to large CB aggregates, breakdown and re-aggregation of the aggregates, breakage of aggregates network under strain. These results may be useful to understand the relationship between CB aggregates network structure and mechanical property of rubber composite. Moreover, they also show that TXM is a valuable technique to study the enhancement mechanism of filled rubber.

## Experimental

### Sample Preparation

The natural rubber used in this study was ribbed smoked sheet (RSS) No.1 from Indonesia. The recipe and cure condition for preparation of the rubber sample are shown in Table 1. In addition to CB, nano copper particles (with diameter of 50 nm) were added to enhance the imaging contrast, though our experimental results demonstrate that the contrast between CB and rubber matrix is sufficient to generate good images with phase contrast imaging technique.

After being mixed with necessary ingredients, the rubber composites were compressed into a 50 μm-thick film with by a compression molding at 143 °C for 15 min for curing. The films were then cut into rectangular shaped specimens with length and width of 15 and 3 mm, respectively, for X-ray imaging experiments. Samples under strain of 0 and 3 were imaged in the current work.

**Table 1**. Recipes and cure conditions of vulcanized natural rubber.

| ingredients | Loading level (phr[a]) |
|---|---|
| natural rubber | 100 |
| stearic acid | 5 |
| ZnO | 2 |
| accelerator TT[b] | 0.5 |
| accelerator DTDM[c] | 0.5 |
| accelerator DM[d] | 0.5 |
| sulfur | 1 |
| CB (N330) | 5.8 |
| copper | 19.3 |
| curing time[e] (min) | 15 |

*a*: Parts by weight per hundred parts of rubber (phr). *b*: Tetramethylthiuram disulfide. *c*: 4,4′-Dithiodimorpholine. *d*: *N*-Cyclohexyl-2-benzothiazolyl sulfenamide. *e*: cure temperature was 143 °C.

## Methods for TXM

The synchrotron radiation TXM experiments were carried out on the 4W1A beamline at the Beijing Synchrotron Radiation Facility (BSRF) as described elsewhere.[31] Briefly, the radiations from wiggler were first monochromatic by double-crystal monochromator. The selected quasi monochromatic X-rays were then focused by an elliptical capillary condenser. Coupled with zone-plate optics, the whole system can perform absorption or phase contrast imaging with X-ray energies from 7 to 11 keV. Images of samples were acquired at tilt angles ranging from -70° to +70° with an interval of 0.5° and then reconstructed into tomograms composed of

6

cubic voxels. In our experiment, phase contrast imaging mode with the X-ray energy

of 8 keV, view field of $60 \times 60$ $\mu m^2$ and a spatial resolution of 100 nm were selected.

Combined with computerized tomography, the spatial information of CB aggregates

in rubber matrix at nanometer scale was obtained in 3D space.
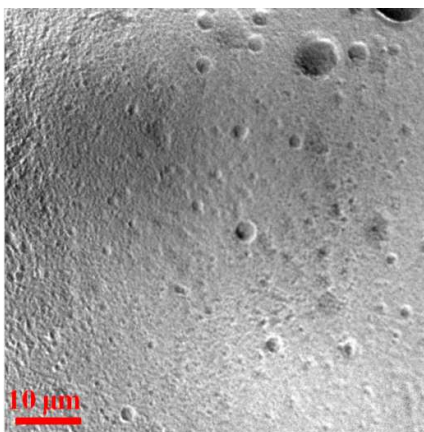
## Results and Discussion



Figure 1. The two-dimensional phase contrast imaging of copper and CB dispersion in natural

rubber matrix.

Figure 1 presents the two-dimensional imaging of copper and CB particles

dispersion in natural rubber matrix. Numerous clusters as well as some large

aggregates could be observed in Figure 1. Diameters of the original CB particles of

N330 and copper particles are about 30 nm and 50 nm, respectively. Therefore single

particle dispersion in rubber matrix is almost inaccessible due to the spatial resolution

limitation of the imaging system. Fortunately, clustering of CB particles into

aggregates with diameters from one hundred to several hundred nanometers, whose

dispersion in rubber matrix can be achieved by imaging with TXM.

In order to evaluate the dispersion differences of copper and CB particles in rubber matrix, three-dimensional images were reconstructed through Amira 5.3.0 software[32]. During the reconstructed process, the thresholding parameters setup is the key factor to discriminate various components in the matrix. In our experiment, we first adjusted the imaging threshold according to the particles dispersing in the two-dimensional projections, and the theoretical volume contents of various components could be calculated according to the results of the 3D segmented and re-constructed imaging. The theoretical contents were compared with the actual copper, carbon black and natural rubber volume contents and the threshold were modified until the theoretical values were very close to the actual values[33], then the thresholding parameters for different components were obtained. In Figure 2, different components were given with different colors for easy distinguishing, where purple zones represent copper aggregates, yellow zones represent CB aggregates, green zones represent natural rubber matrix and red zones represent nano pores, respectively. In X-ray imaging, only structures with size larger than the spatial resolution of the imaging system (100 nm) can be obtained. In our experiment, the ingredients in the rubber are not much little, which make it difficult to form large clusters more than 100 nm, also some ingredients may be existed at molecule level, so the other ingredients give little influence on the imaging result and ignore them during imaging 3D reconstruction. As can be seen in Figure 2, the distributions of different components can be distinguished obvious in the natural rubber matrix and the volume fractions for different components are evaluated quantitatively as listed in Table 2. As shown in

Figure 2, the CB aggregates can be easily distinguished from the natural rubber matrix,

though the density difference between CB and natural rubber is relatively small.
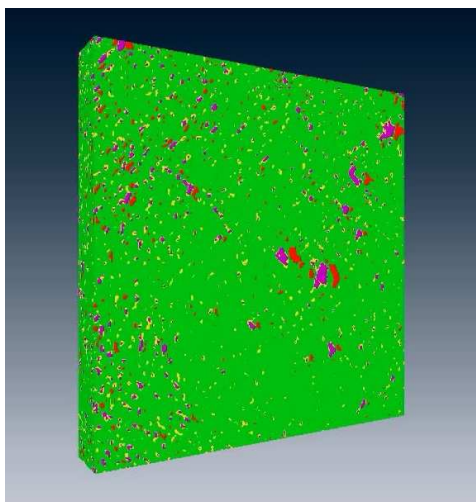


Figure 2. The dispersion of different components in the 3D space where purple zones represent

copper aggregates, yellow zones represent CB aggregates, green zones represent natural rubber

matrix and red zones represent nano pores, respectively.

Table 2. The volume fractions of different components in three different rubber composites

| component | volumes | volumes from formulation |
|---|---|---|
| copper | 2.30% | 1.78% |
| CB | 3.10% | 2.64% |
| natural rubber | 93.20% | 95.58% |
| nano pores | 1.50% | 0 |

The 3D dispersions of CB aggregates and nano pores in the rubber matrix at

strain of 3 are obtained from reconstruction and presented in Figure 3. As shown in

Figure 3, the 3D dispersion of CB aggregates in rubber matrix is not homogeneous

with some spots filled by highly concentrated aggregates. Furthermore, coincidence of

large aggregates and large pores concomitant with inhomogeneous 3D dispersion of

nano pores in the rubber matrix indicates that CB aggregates lead to stress

concentration due to the exist of large pores[34, 35]. In other words, CB network indeed

takes large external load and plays a key role in the mechanical performance of

rubber/filler composite. Naturally, inhomogeneous distribution of CB aggregates may

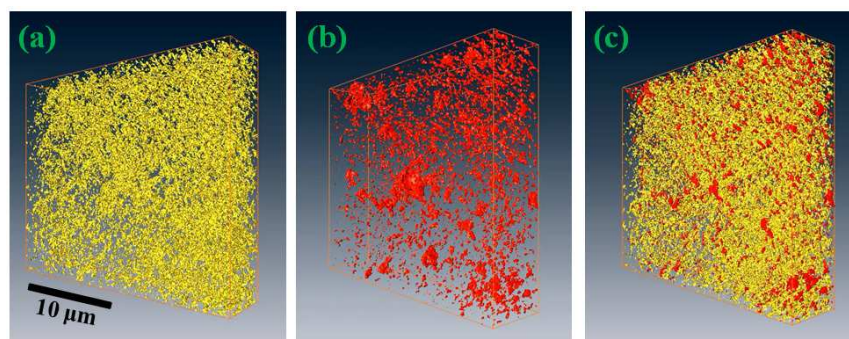also worsen the mechanical properties due to stress concentration.



Figure 3. 3D dispersions of different components in the natural rubber matrix at strain of 3: (a) CB

aggregates; (b): nano pores; (c): the summary of CB aggregates and nano pores.

In order to quantitatively describe the enhancement mechanism for CB filled

natural rubber, crucial parameters such as the size of aggregates and the

inter-aggregate distance are derived from 3D images for CB dispersion in the rubber

matrix at different strains. Sample slices of the 3D images are presented in Figure 4,

where the aggregates are highlighted in order to easy analyses. The size of aggregate

and inter-aggregate distance are obtained through the pixels analysis of slices, namely

the number of pixels in red zones and adjacent red zones, similar to previous

researcher[20]. Then the frequency of certain size (inter-aggregate distance) is obtained

through the ratio of certain size's (inter-aggregate distance's) number and the whole

number of different sizes (inter-aggregate distances). Based on these slices, the frequency of different sizes and inter-aggregate distances at strain of 0 and 3 are obtained and presented in Figures 5 and 6, respectively. At strain of 0, Figure 5 shows very similar value for the average size of aggregates (the average size $\xi_h = \sum \xi_i f_i$, $\xi_i$ and $f_i$ are the size and frequency of certain aggregate, similar method was used for calculating the average inter-aggregate distance in the following part) parallel and perpendicular to the stretching direction suggesting the existence of spherical or isotropic aggregates. Furthermore the sizes of aggregates obtained are similar to the previous U-SAXS results[36, 37]. In addition to the frequency of similar-sized aggregates drops monotonously with the increase of size. Interestingly, at strain of 3 the frequency of similar-sized aggregates does not follow a monotonic decreasing trend but oscillates with the increase of aggregate size as shown by the aggregates size distribution plot in Figure 5 (c) and (d). This strong oscillation is certainly generated by stretching and the underlying mechanism may be due to stretch-induced elongation, breakage and re-aggregation of CB aggregates, which can be found in the local magnifying image presented in Figure 7 (the 3D local magnifying video can be seen in Supplement Information). Such a phenomenon is expected to generate more aggregates with smaller sizes, especially along the stretching direction, while this effect may be slightly weaker perpendicular to stretching direction due to shear force. The agreement between the above expectation and the experimental results in Figure 5 (c) and (d) supports the proposed mechanism of stretch-induced breakage and re-aggregation of CB aggregates.
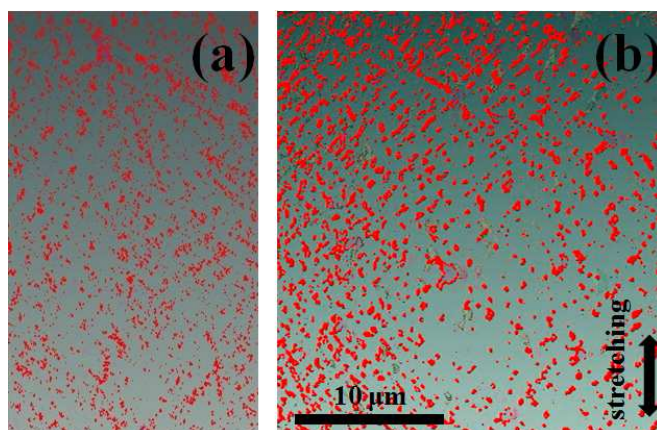
Figure 4. The slices of the three dimensional imaging for CB aggregates in the natural rubber

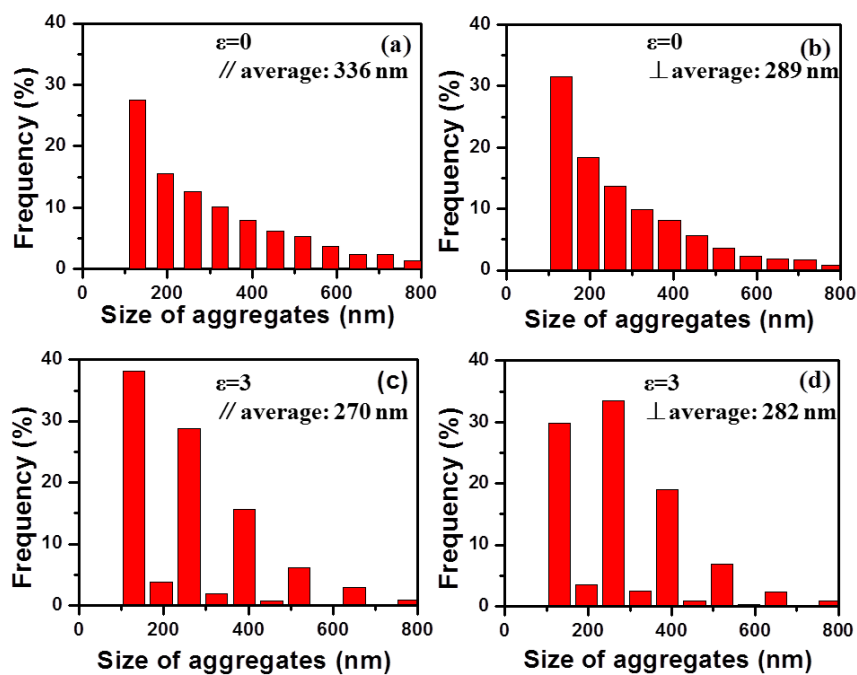matrix before stretched (a) and after stretched to strain of 3 (b).



Figure 5. The aggregates size distribution parallel (a, c) and perpendicular (b, d) to the stretching

direction before stretched (a, b) and after stretched to strain of 3 (c, d).


The inter-aggregate distances with and without strain are presented in Figure 6

and the average distances are in the range of 1.2 to 1.4 μm. Before stretching, the

frequency of similar-inter-aggregate distance shows a decay trend along with the

12

inter-aggregate distance increasing. On the other hand, under strain of 3 a maximum

exists in the frequency- inter-aggregate distance plot, which indicates a most suitable

inter-aggregate distance exists after stretched to strain 3. Interestingly, the most

suitable inter-aggregate distance along stretching direction is about 700 nm, which is

about 200 nm larger than that perpendicular to the stretching direction. Such a

discrepancy is mainly due to the different effects of tensile and shear forces in

different directions. Similar to the dispersion of aggregates size, a strong oscillation of

the inter-aggregate distance distribution plot is also observed by increasing the

inter-aggregate distance. This can also be attributed to stretch-induced breakage and

re-aggregation of CB aggregates as discussed above on the dispersion of aggregate
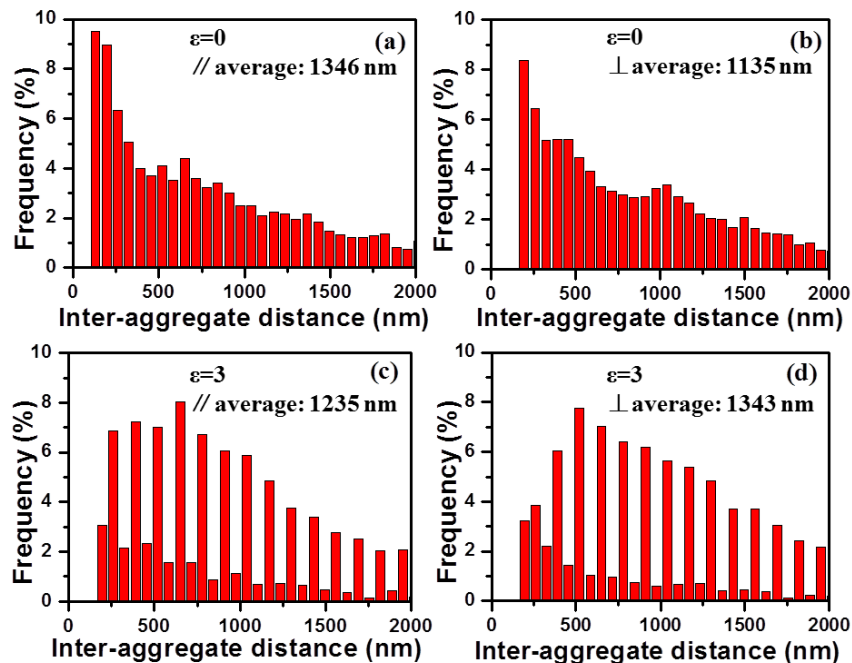
sizes.



Figure 6. The inter-aggregate distance distribution parallel (a, c) and perpendicular (b, d) to the

stretching direction before stretched (a, b) and after stretched to strain of 3 (c, d).
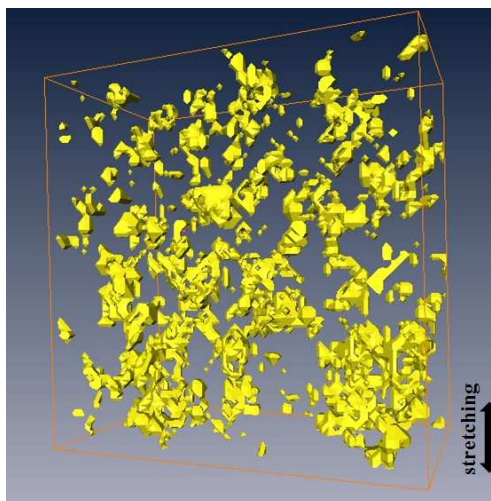
Figure 7. The local magnifying image of the morphology for CB aggregates at the strain of 3.

Stretch-induced breakage and re-aggregation of CB aggregates modify the network structure such as the size of aggregates and inter-aggregate distance, which is expected to affect the mechanical property of filled natural rubber composite. For a quantitative estimation, we borrow the soft-hard double network model[38] developed by Okumura to calculate the enhancement factor of hard network at different strains. In current context, the CB aggregates and natural rubber matrix are assigned as hard and soft networks, respectively. The fracture energy enhancement factor of CB filled natural rubber can be defined as

$$\lambda \sim \frac{\mu_h}{\mu_s a_s} \frac{\xi_h^3}{\xi_s^2}. \tag{1}$$

Here, $\mu_h$ and $\mu_s$ are the modulus for aggregates and natural rubber matrix, respectively; $a_s$ is the characteristic microscopic size of defect or Griffith cavities for the rubber matrix; $\xi_h$ and $\xi_s$ are the size of aggregates and inter-aggregate distance parallel to the stretching direction, respectively. Thus the ratio of the contribution of CB network to the mechanical property at strain of 3 and 0 can be calculate as

$$\frac{\lambda_3}{\lambda_0} = \frac{\xi_{3h}^3}{\xi_{0h}^3} \times \frac{\xi_{0s}^2}{\xi_{3s}^2}. \tag{2}$$

With $\xi_{0h}$=336 nm, $\xi_{0s}$=1346 nm, $\xi_{3h}$=270 nm, $\xi_{3s}$=1235 nm derived from imaging, $\lambda_3 / \lambda_0 = 0.6138$ is obtained. The reduction of enhancement factor at strain of 3 suggests that stretch-induced breakage and re-aggregation of CB aggregates depress the contribution of CB network to the mechanical property of rubber composite parallel to the stretching direction. This is a direct experimental evidence for the structural origin of Payne effect,[12] where stretch-induced breakage of filler network is responsible for the reduction of modulus.

## Conclusions

The network structure of CB aggregates in rubber matrix is studied with synchrotron radiation TXM at different strains. Three dimensional images provide information including the size of aggregates, inter-aggregate distance and the nano pores. Statistical analyses on the three dimensional images shows that stretch-induced breakdown and reaggregation of the aggregates occur and lead to a reduction of the contribution of CB aggregates on the mechanical property of rubber composite. Additionally, pores are generated around the large aggregates of CB, which indicates that CB aggregates serve as stress concentrator. Current work demonstrates that TXM is an effective technique to study filler network under quiescent and deformation conditions, which may contribute to the understanding of the enhancement mechanism of fillers in composite materials.

## Acknowledgement

RSC Advances Accepted Manuscript

16

# References

1. H. H. Cai, S. D. Li, G. R. Tian, H. B. Wang and J. H. Wang, *J. Appl. Polym. Sci.*, 2003, **87**, 982-985.

2. R. Pérez-Aparicio, A. Vieyres, P.-A. Albouy, O. Sanséau, L. Vanel, D. R. Long and P. Sotta, *Macromolecules*, 2013, **46**, 8964-8972.

3. S. Joly, G. Garnaud, R. Ollitrault, L. Bokobza and J. E. Mark, *Chem. Mater.*, 2002, **14**, 4202-4208.

4. S. Trabelsi, P. A. Albouy and J. Rault, *Macromolecules*, 2003, **36**, 9093-9099.

5. J. Rault, J. Marchal, P. Judeinstein and P. A. Albouy, *Macromolecules*, 2006, **39**, 8356-8368.

6. A. P. Meera, S. Said, Y. Grohens, A. S. Luyt and S. Thomas, *Ind. Eng. Chem. Res.*, 2009, **48**, 3410-3416.

7. S. Poompradub, M. Tosaka, S. Kohjiya, Y. Ikeda, S. Toki, I. Sics and B. S. Hsiao, *J. Appl. Phys.*, 2005, **97**, 103529.

8. L. H. Cohan and R. Spielman, *Ind. Eng. Chem.*, 1948, **40**, 2204-2210.

9. J. Carretero-Gonzalez, H. Retsos, R. Verdejo, S. Toki, B. S. Hsiao, E. P. Giannelis and M. A. Lopez-Manchado, *Macromolecules*, 2008, **41**, 6763-6772.

10. A. R. Payne, *J. Appl. Polym. Sci.*, 1962, **6**, 368-372.

11. A. R. Payne, *J. Appl. Polym. Sci.*, 1962, **6**, 57-63.

12. A. R. Payne, *J. Appl. Polym. Sci.*, 1960, **3**, 127-127.

13. S. Kohjiya, A. Kato and Y. Ikeda, *Prog. Polym. Sci.*, 2008, **33**, 979-997.

14. S. Toki, C. Burger, B. S. Hsiao, S. Amnuaypornsri, J. Sakdapipanich and Y. Tanaka, *J. Polym. Sci., Part B: Polym. Phys.*, 2008, **46**, 2456-2464.

15. Y. Zhang, S. Ge, B. Tang, T. Koga, M. H. Rafailovich, J. C. Sokolov, D. G. Peiffer, Z. Li, A. J. Dias, K. O. McElrath, M. Y. Lin, S. K. Satija, S. G. Urquhart, H. Ade and D. Nguyen, *Macromolecules*, 2001, **34**, 7056-7065.

16. P. Bindu and S. Thomas, *J. Phys. Chem. B*, 2013, **117**, 12632-12648.

17. A. P. Meera, S. Said, Y. Grohens and S. Thomas, *J. Phys. Chem. C*, 2009, **113**, 17997-18002.

18. H. Angellier, S. Molina-Boisseau, L. Lebrun and A. Dufresne, *Macromolecules*, 2005, **38**, 3783-3792.

19. K. Brüning, K. Schneider, S. V. Roth and G. Heinrich, *Macromolecules*, 2012, **45**, 7914-7919.

20. F. Yatsuyanagi, N. Suzuki, M. Ito and H. Kaidou, *Polymer*, 2001, **42**, 9523-9529.

21. Y. Ikeda, A. Katoh, J. Shimanuki and S. Kohjiya, *Macromol. Rapid Commun.*, 2004, **25**, 1186-1190.

22. G. P. Baeza, A.-C. Genix, C. Degrandcourt, J. Gummel, A. Mujtaba, K. Saalwächter, T. Thurn-Albrecht, M. Couty and J. Oberdisse, *ACS Macro Lett.*, 2014, **3**, 448-452.

23. A. Kato, T. Suda, Y. Ikeda and S. Kohjiya, *J. Appl. Polym. Sci.*, 2011, **122**, 1300-1315.

24. F. Ehrburger-Dolle, M. Hindermann-Bischoff, F. Livet, F. Bley, C. Rochas and E. Geissler, *Langmuir*, 2000, **17**, 329-334.

25. T. Koga, T. Hashimoto, M. Takenaka, K. Aizawa, N. Amino, M. Nakamura, D. Yamaguchi and S. Koizumi, *Macromolecules*, 2007, **41**, 453-464.

26. Y. Tian, W. Li, J. Chen, L. Liu, G. Liu, A. Tkachuk, J. Tian, Y. Xiong, J. Gelb, G. Hsu and W. Yun, *Rev. Sci. Instrum.*, 2008, **79**, 103708.

27. J. Li, A. P. Hitchcock, H. D. H. Stöver and I. Shirley, *Macromolecules*, 2009, **42**, 2428-2432.

28.    L. Bertrand, L. Robinet, M. Thoury, K. Janssens, S. Cohen and S. Schöder, *Appl. Phys. A*, 2012, **106**, 377-396.

29.    Q. Dong, J. Zhang, J. Dong, Y. Dai, F. Bian, H. Xie, Y. Lu and B. Sun, *Mater. Lett.*, 2011, **65**, 3295-3297.

30.    R. Liu, X. Yin, H. Li, Q. Shao, P. York, Y. He, T. Xiao and J. Zhang, *Int. J. Pharm.*, 2013, **445**, 125-133.

31.    P. P. Zhu, J. Y. Wang, Q. X. Yuan, W. X. Huang, H. Shu, B. Gao, T. D. Hu and Z. Y. Wu, *Appl. Phys. Lett.*, 2005, **87**, 264101.

32.    The TGS Co. home page, http://www.tgs.com.

33.    R. Flückiger, F. Marone, M. Stampanoni, A. Wokaun and F. N. Büchi, *Electrochim. Acta*, 2011, **56**, 2254-2262.

34.    J. Bagdahn, W. N. Sharpe and O. Jadaan, *J. Micromech. Syst*, 2003, **12**, 302-312.

35.    H. Liebowitz, *Fracture;*, Academic Press, 1992.

36.    T. P. Rieker, M. Hindermann-Bischoff and F. Ehrburger-Dolle, *Langmuir*, 2000, **16**, 5588-5592.

37.    T. P. Rieker, S. Misono and F. Ehrburger-Dolle, *Langmuir*, 1999, **15**, 914-917.

38.    K. Okumura, *EPL* 2004, **67**, 470-476.